

# Scintillation and Thermally Stimulated Luminescence Properties of Sn-doped CaO–B<sub>2</sub>O<sub>3</sub>–SiO<sub>2</sub> Glasses

Hiroyuki Fukushima,\* Daiki Shiratori, Daisuke Nakauchi,  
Takumi Kato, Noriaki Kawaguchi, and Takayuki Yanagida

Division of Materials Science, Nara Institute of Science and Technology,  
8916-5 Takayama-Cho, Ikoma, Nara 630-0192, Japan

(Received October 14, 2021; accepted November 5, 2021)

**Keywords:** scintillation, TSL, photoluminescence, glass, Sn-doped phosphor

Sn-doped 30CaO–50B<sub>2</sub>O<sub>3</sub>–20SiO<sub>2</sub> glass samples were prepared by the conventional melt-quenching method, and the photoluminescence (PL), scintillation, and thermally stimulated luminescence (TSL) properties were investigated. The PL and scintillation spectra of the Sn-doped samples exhibited a broad luminescence band with a maximum at 410 nm due to a T<sub>1</sub>→S<sub>0</sub> transition of Sn<sup>2+</sup>, and the PL and scintillation decay time constants were approximately 5.7 and 6.3 μs, respectively. The Sn-doped samples exhibited TSL glow peaks at ~80 and 280 °C after X-ray irradiation, and the TSL intensity increased monotonically with the X-ray irradiation dose from 10 to 10000 mGy.

## 1. Introduction

Scintillators and storage-type phosphors have been utilized for ionizing radiation detectors. Scintillators convert instantaneously absorbed energy of ionizing radiation to low-energy photons, and their application fields are medical imaging,<sup>(1–4)</sup> luggage inspection,<sup>(5)</sup> resource exploration,<sup>(6)</sup> and environmental monitoring.<sup>(7,8)</sup> In contrast, storage-type phosphors store temporarily absorbed energy of ionizing radiation in the form of carrier trapping, and then the emission is observed when the stored carriers are stimulated by heat or light. Such emissions are known as thermally stimulated luminescence (TSL) or optically stimulated luminescence (OSL). The TSL or OSL intensity depends on the absorbed ionizing radiation dose; thus, storage-type phosphors are applied for personal dose monitoring.<sup>(9–11)</sup> Scintillators and storage-type phosphors have been developed by different research communities, and an inverse relationship between the scintillation intensity and the TSL or OSL intensity has been reported recently.<sup>(12,13)</sup> In other words, when the scintillation intensity is high, the TSL or OSL intensity is low.

To investigate scintillation, TSL, and OSL properties, many materials such as single crystals,<sup>(14–22)</sup> ceramics,<sup>(23–29)</sup> and glasses<sup>(30–34)</sup> have been employed. The detection efficiency of scintillators and storage-type phosphors depends on the volume of the material; thus, transparent materials are preferable to detect emissions generated inside materials. Among the material

---

\*Corresponding author: e-mail: [fukushima.hiroyuki.ex8@ms.naist.jp](mailto:fukushima.hiroyuki.ex8@ms.naist.jp)  
<https://doi.org/10.18494/SAM3691>

forms, glasses are advantageous for scintillators and storage-type phosphors due to their high transparency, low production cost, and high chemical durability. To date, only two types of glasses, Li glass<sup>(35,36)</sup> as a scintillator and Ag-doped phosphate glass<sup>(11,37)</sup> as a storage-type phosphor, are commercially available, and there is considerable scope for the study of glasses.

Borosilicate glasses have high chemical durability and transparency, making them attractive for use as scintillators and storage-type phosphors. So far, rare-earth-doped CaO–B<sub>2</sub>O<sub>3</sub>–SiO<sub>2</sub> glasses have been studied for use in LEDs,<sup>(38–40)</sup> and the glasses exhibited a relatively high photoluminescence (PL) quantum yield (*QY*). In previous studies, Sn-doped silicate, borate, and borosilicate glasses demonstrated a high PL *QY* and a broad luminescence band at ~400 nm, making them suitable for radiation measurement with a conventional photomultiplier tube, and strong scintillation and TSL intensity were observed.<sup>(41–44)</sup> In this study, the PL, scintillation, and TSL properties of Sn-doped 30CaO–50B<sub>2</sub>O<sub>3</sub>–20SiO<sub>2</sub> glasses were investigated.

## 2. Materials and Methods

Sn-doped 30CaO–50B<sub>2</sub>O<sub>3</sub>–20SiO<sub>2</sub> glass samples were prepared by the melt-quenching method. CaO (99.99%), B<sub>2</sub>O<sub>3</sub> (99.999%), SiO<sub>2</sub> (99.99%), and SnO<sub>2</sub> (99.99%) were used as starting materials and mixed uniformly using a mortar and pestle. The nominal doped concentrations of Sn were 0.01, 0.05, 0.1, 0.5, 1, and 3%. The mixed powders were loaded into an alumina crucible and then placed in an electric furnace at 1400 °C for 30 min in air. The melt was poured onto a stainless plate heated at 300 °C and then quickly quenched using another stainless plate.

The absorption spectra were measured with a spectrometer (V670, JASCO) in the wavelength range of 190–2700 nm. The PL excitation and emission contour map and PL *QY* were measured with a spectrometer (C11347-01, Hamamatsu Photonics). The PL decay curves were evaluated with a spectrometer (C11367, Hamamatsu Photonics).

The X-ray-induced scintillation spectra and decay curves were measured with laboratory-made setups.<sup>(45,46)</sup> A tube voltage of 80 kV and current of 1.2 mA were supplied during the measurement of the X-ray-induced scintillation spectra.

The TSL glow curves were measured with a TSL reader (TL-2000, Nanogray) after X-ray irradiation.<sup>(47)</sup> The measurement range was 50–490 °C and the heating rate was 1 °C/s.

## 3. Results and Discussion

Figure 1 shows the prepared Sn-doped CaO–B<sub>2</sub>O<sub>3</sub>–SiO<sub>2</sub> glass samples after polishing. The thickness of these samples was approximately 1 mm. All the samples were colorless and transparent. The weights of the samples are listed in Table 1. The absorption spectra of the glass samples in the range from 190 to 2700 nm are shown in Fig. 2. Here, data for undoped glass are also plotted for comparison of the absorption band. All the Sn-doped glass samples exhibited an absorption band around 230–300 nm, and the absorption wavelength was shifted to the long-wavelength side with increasing concentration of Sn. The redshift of the absorption edge is considered to be due to the change in the local coordination environment and valence state of Sn with increasing concentration of doped Sn.<sup>(42)</sup> In previous reports on Sn-doped glasses, the

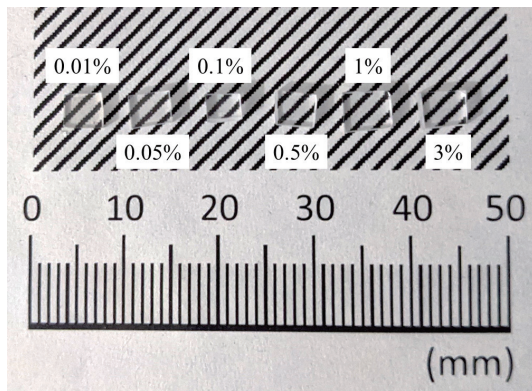


Fig. 1. Photograph of Sn-doped CaO–B<sub>2</sub>O<sub>3</sub>–SiO<sub>2</sub> glasses.

Table 1  
Weights of Sn-doped CaO–B<sub>2</sub>O<sub>3</sub>–SiO<sub>2</sub> glasses.

	Weight (mg)
0.01% Sn	40.9
0.05% Sn	50.6
0.1% Sn	44.4
0.5% Sn	51.1
1% Sn	69.0
3% Sn	56.2

absorption around 230–300 nm was assigned as an  $S_0 \rightarrow S_1$  excitation of  $\text{Sn}^{2+}$ .<sup>(43,44)</sup> The undoped and Sn-doped glass samples exhibited absorption at 200 nm. The absorption edge was shifted slightly to the long-wavelength side with increasing concentration of Sn. The baseline of the 0.1% Sn-doped sample was higher than those of the other samples, and the difference was considered to originate from the different sample surface conditions. The absorption below 280 nm was similar for all Sn concentrations and appeared to be saturated. In this study, the thickness of the glass samples was approximately 1 mm; thus, the absorption spectra should be measured using thinner samples to investigate the plateau in the future.

Figure 3 shows the PL excitation and emission contour map of the 3% Sn-doped CaO–B<sub>2</sub>O<sub>3</sub>–SiO<sub>2</sub> glass sample as a representative sample. The peak emission wavelength was 410 nm under an excitation wavelength of 310 nm. The excitation wavelength corresponded to the absorption wavelength as shown in Fig. 2; thus, the excitation originated from an  $S_0 \rightarrow S_1$  transition of  $\text{Sn}^{2+}$ . Some other Sn-doped glass materials also show similar excitation spectra.<sup>(42,44,48)</sup> A broad emission band with a peak emission wavelength around 410 nm was observed in the Sn-doped glass materials, and the origin of the emission was ascribed to a  $T_1 \rightarrow S_0$  transition of  $\text{Sn}^{2+}$ .<sup>(43,44)</sup> The obtained PL QYs of the Sn-doped glass samples are listed in Table 2. PL QY increased with increasing concentration of Sn, and the maximum PL QY of 41.9% was obtained for the 3% Sn-doped sample. Previously reported PL QYs in Sn-doped aluminoborate and silicophosphate glass samples also exhibited similar values.<sup>(48,49)</sup> Figure 4 shows the PL decay curves of Sn-doped CaO–B<sub>2</sub>O<sub>3</sub>–SiO<sub>2</sub> glass samples, which were measured for further investigation of the origin of the emission. The observed PL decay curves were fitted by a single exponential decay function, and the obtained PL decay constants of all the samples are listed in Table 2. The obtained PL decay constants were  $\sim 5.7 \mu\text{s}$ , as typically observed in Sn-doped glasses.<sup>(43,44,48,49)</sup> From the results of the PL decay constants and the emission wavelength, the origin of the emission of 410 nm was ascribed to a  $T_1 \rightarrow S_0$  transition of  $\text{Sn}^{2+}$ .

Figure 5 shows the X-ray-induced scintillation spectra of the Sn-doped CaO–B<sub>2</sub>O<sub>3</sub>–SiO<sub>2</sub> glass samples. The scintillation spectra had a similar shape to the PL spectra, and

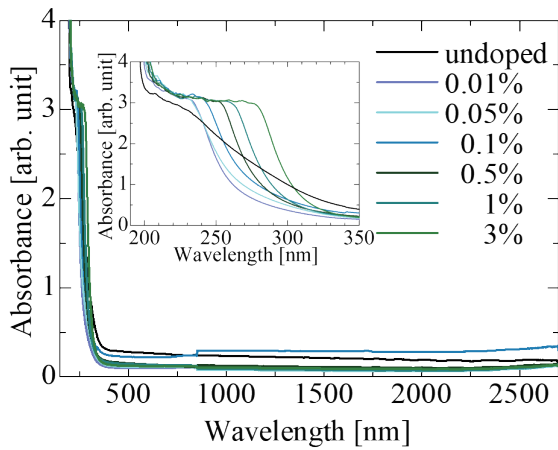


Fig. 2. (Color online) Absorption spectra of undoped and Sn-doped CaO–B<sub>2</sub>O<sub>3</sub>–SiO<sub>2</sub> glasses in the range from 190 to 2700 nm. The inset shows enlarged spectra in the range from 190 to 350 nm.

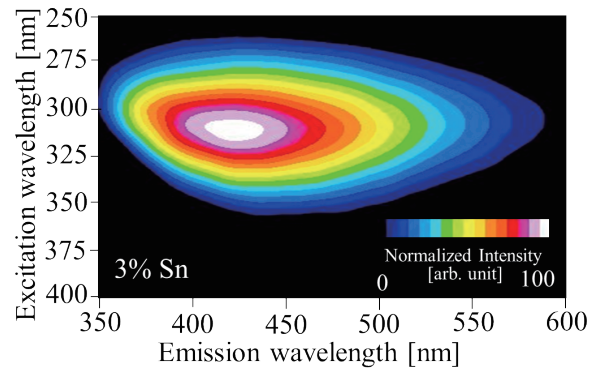


Fig. 3. (Color online) PL excitation and emission contour map of 3% Sn-doped CaO–B<sub>2</sub>O<sub>3</sub>–SiO<sub>2</sub> glass.

Table 2  
PL *QY*s and PL decay constants of Sn-doped CaO–B<sub>2</sub>O<sub>3</sub>–SiO<sub>2</sub> glasses.

	PL <i>QY</i> (%)	PL decay constant ( $\mu$ s)
0.01% Sn	10.7	5.7
0.05% Sn	12.8	5.8
0.1% Sn	18.4	5.7
0.5% Sn	36.5	5.7
1% Sn	40.8	5.7
3% Sn	41.9	5.7

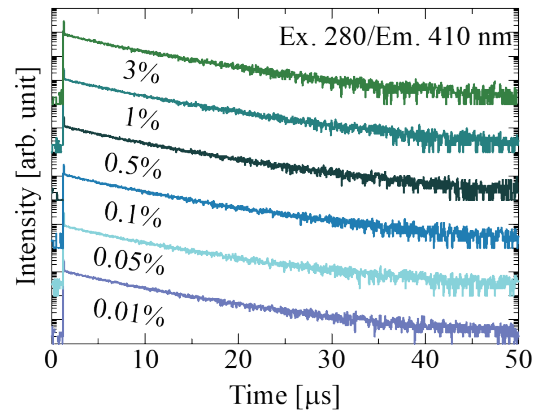


Fig. 4. (Color online) PL decay curves of Sn-doped CaO–B<sub>2</sub>O<sub>3</sub>–SiO<sub>2</sub> glasses monitored at 410 nm under 280 nm excitation.

the intensity increased with increasing concentration of Sn. The intensity of the scintillation spectrum depended on PL *QY*. On the other hand, the scintillation intensity of the 3% Sn-doped sample was higher than that of the 1% Sn-doped sample, although the PL *QY*s of both samples were almost the same. The scintillation process involves an energy conversion process and an energy migration process before emission at a luminescence center.<sup>(50)</sup> Judging from the absorption edge at 200 nm, as shown in Fig. 2, the optical bandgaps of the 1 and 3% Sn-doped samples were almost the same; thus, the energy conversion efficiency was considered to be similar. PL *QY* for the 3% Sn-doped sample was almost the same as that for the 1% Sn-doped sample, although the scintillation intensity of the 3% Sn-doped sample was higher than that of the 1% Sn-doped sample; thus, the energy migration efficiency of the 3% Sn-doped sample was considered to be higher than that of the 1% Sn-doped sample.

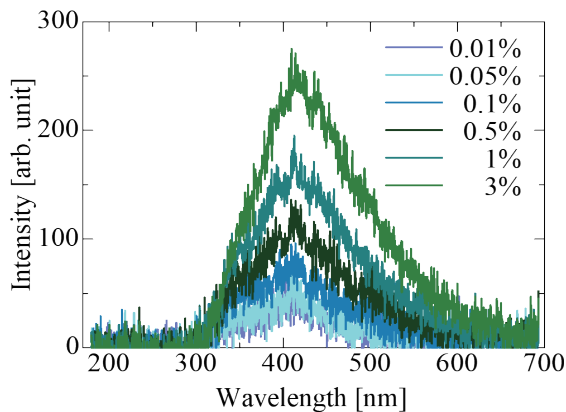


Fig. 5. (Color online) X-ray-induced scintillation spectra of Sn-doped CaO–B<sub>2</sub>O<sub>3</sub>–SiO<sub>2</sub> glasses.

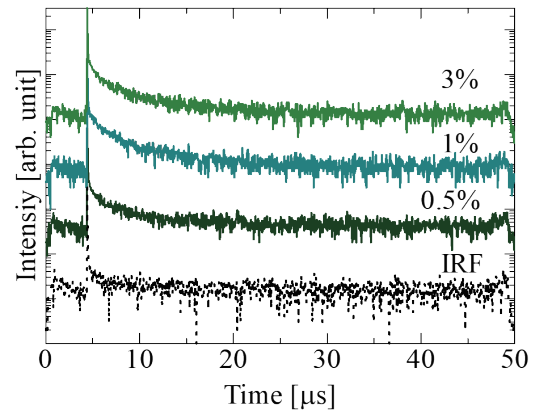


Fig. 6. (Color online) X-ray-induced scintillation decay curves of 0.5, 1, and 3% Sn-doped CaO–B<sub>2</sub>O<sub>3</sub>–SiO<sub>2</sub> glasses.

Figure 6 shows the X-ray-induced scintillation decay curves of the 0.5, 1, and 3% Sn-doped CaO–B<sub>2</sub>O<sub>3</sub>–SiO<sub>2</sub> glass samples. For the other samples, only signals similar to the instrumental response function (IRF) were obtained due to the low scintillation intensity. The observed scintillation decay curves were approximated by a sum of two exponential decay functions. Table 3 lists the obtained scintillation decay constants  $\tau_1$  and  $\tau_2$ . The origin of the decay corresponding to  $\tau_1$  was ascribed to the IRF, and the values of  $\tau_2$  were similar to those for the PL; thus, the origin of the decay corresponding to  $\tau_2$  was ascribed to a  $T_1 \rightarrow S_0$  transition of Sn<sup>2+</sup>.

Figure 7 shows the TSL glow curves of the Sn-doped CaO–B<sub>2</sub>O<sub>3</sub>–SiO<sub>2</sub> glass samples after 1000 mGy X-ray irradiation. Broad TSL glow peaks appeared at  $\sim 80$  and  $280$  °C. The TSL peak temperature of  $\sim 280$  °C was higher than room temperature; thus, the TSL peak at  $\sim 280$  °C was considered to be less susceptible to fading than that observed at  $\sim 80$  °C. The TSL intensity decreased with increasing concentration of Sn; however, the TSL intensity of the 0.1% Sn-doped sample was higher than that of the 0.05% Sn-doped sample. Although the TSL intensity should depend on the weight of the sample, the weight of the 0.1% Sn-doped sample was greater than that of the 3% Sn-doped sample. The TSL intensity also depends on the probability of capturing electron-hole pairs at trapping centers;<sup>(51)</sup> thus, the 0.1% Sn-doped sample was considered to have a higher TSL efficiency than the 0.05% Sn-doped sample. A complementary relationship was observed between the TSL and scintillation intensities.<sup>(12,13)</sup> Figure 8 shows the X-ray dose response functions of the Sn-doped CaO–B<sub>2</sub>O<sub>3</sub>–SiO<sub>2</sub> glass samples. In this evaluation, the vertical axis indicates the integrated TSL intensity in the range from 50 to 490 °C. The TSL intensity of the 3% Sn-doped sample exhibited no change with varying X-ray irradiation dose; thus, no data for this sample were plotted in Fig. 8. For the other samples, the integrated TSL intensity increased monotonically with the X-ray irradiation dose. The lowest detection limit of the Sn-doped samples was 10 mGy, and the 1% Sn-doped sample showed a detection limit of 100 mGy due to its low TSL intensity. The lowest detection

Table 3

X-ray-induced scintillation decay constants of Sn-doped CaO–B<sub>2</sub>O<sub>3</sub>–SiO<sub>2</sub> glasses and IRF.

	$\tau_1$ ( $\mu$ s)	$\tau_2$ ( $\mu$ s)
IRF	0.7	N/A
0.5% Sn	0.4	6.3
1% Sn	0.7	6.3
3% Sn	0.6	6.4

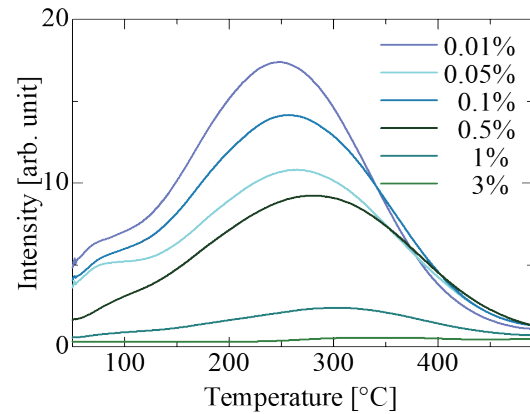


Fig. 7. (Color online) TSL glow curves of Sn-doped CaO–B<sub>2</sub>O<sub>3</sub>–SiO<sub>2</sub> glasses after 1000 mGy irradiation.

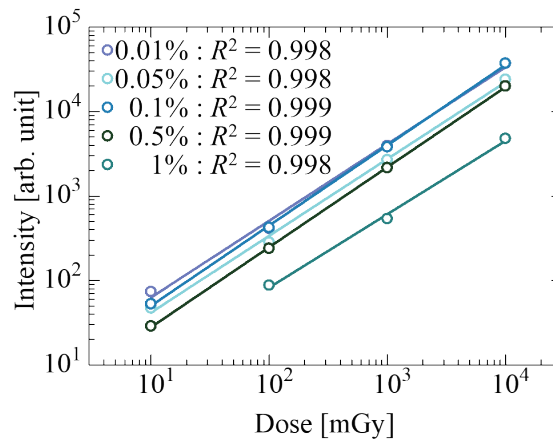


Fig. 8. (Color online) TSL dose response functions of Sn-doped CaO–B<sub>2</sub>O<sub>3</sub>–SiO<sub>2</sub> glasses.

limit of 10 mGy was worse than those for other glasses,<sup>(44,52,53)</sup> and it was still insufficient for a personal dosimeter. To improve the lowest detection limit, further investigation with lower concentrations of Sn is needed.

#### 4. Conclusions

Sn-doped glass samples were prepared by the conventional melt-quenching method, and their PL, scintillation, and TSL properties were investigated. The PL excitation and emission contour map exhibited a broad emission band due to a  $T_1 \rightarrow S_0$  transition of Sn<sup>2+</sup>, and PL  $QY$  increased with increasing concentration of Sn. Scintillation spectra exhibited a similar emission feature to the PL, and the scintillation intensity also increased with increasing concentration of Sn. TSL glow peaks appeared at  $\sim 80$  and  $280$  °C after X-ray irradiation, and the TSL intensity decreased with increasing concentration of Sn. A complementary relationship was

observed between scintillation intensity and TSL intensity. Judging from the results, the optimum concentrations of Sn for scintillation and TSL were 3 and 0.01%, respectively.

### Acknowledgments

This work was supported by Grants-in-Aid for Scientific Research B (19H03533, 21H03733, and 21H03736) and Early-Career Scientists (20K20104) from Japanese Society of Applied Physics (JSPS). Foundation from JST A-STEP (JPMJTM20FP), Cooperative Research Project of the Research Center for Biomedical Engineering, Nippon Sheet Glass Foundation, SEI Group CSR Foundation, TEPCO Memorial Foundation, and KRF Foundation, and Murata Science Foundation are also acknowledged.

### References

- 1 T. K. Lewellen: *Phys. Med. Biol.* **53** (2008) R287.
- 2 C. L. Melcher: *J. Nucl. Med.* **41** (2000) 1051.
- 3 C. W. E. Van Eijk: *Phys. Medica* **12** (1996) 23.
- 4 W. Rossner and B. C. Grabmaier: *J. Lumin.* **48–49** (1991) 29.
- 5 G. Harding: *Radiat. Phys. Chem.* **71** (2004) 869.
- 6 T. Yanagida, Y. Fujimoto, S. Kurosawa, K. Kamada, H. Takahashi, Y. Fukazawa, M. Nikl, and V. Chani: *Jpn. J. Appl. Phys.* **52** (2013)
- 7 S. Kishimoto and T. Yamamoto: *Nucl. Instrum. Methods Phys. Res., Sect. A* **508** (2003) 425.
- 8 K. Watanabe, T. Yanagida, K. Fukuda, A. Koike, T. Aoki, and A. Uritani: *Sens. Mater.* **27** (2015) 269.
- 9 J. Azorin Nieto: *Appl. Radiat. Isot.* **117** (2016) 135.
- 10 S. W. S. McKeever, M. Akselrod, and B. G. Markey: *Radiat. Prot. Dosimetry* **65** (1996) 267.
- 11 Y. Miyamoto, Y. Takei, H. Nanto, T. Kurobori, A. Konnai, T. Yanagida, A. Yoshikawa, Y. Shimotsuma, M. Sakakura, K. Miura, K. Hirao, Y. Nagashima, and T. Yamamoto: *Radiat. Meas.* **46** (2011) 1480.
- 12 T. Yanagida: *J. Lumin.* **169** (2016) 544.
- 13 T. Yanagida, Y. Fujimoto, K. Watanabe, K. Fukuda, N. Kawaguchi, Y. Miyamoto, and H. Nanto: *Radiat. Meas.* **71** (2014) 162.
- 14 P. Kantuptim, H. Fukushima, H. Kimura, D. Nakauchi, T. Kato, M. Koshimizu, N. Kawaguchi, and T. Yanagida: *Sens. Mater.* **33** (2021) 2195.
- 15 D. Nakauchi, T. Kato, N. Kawaguchi, and T. Yanagida: *Sens. Mater.* **33** (2021) 2203.
- 16 H. Fukushima, M. Akatsuka, H. Kimura, D. Onoda, D. Shiratori, D. Nakauchi, T. Kato, N. Kawaguchi, and T. Yanagida: *Sens. Mater.* **33** (2021) 2235.
- 17 M. Akatsuka, H. Kimura, D. Onoda, D. Shiratori, D. Nakauchi, T. Kato, N. Kawaguchi, and T. Yanagida: *Sens. Mater.* **33** (2021) 2243.
- 18 T. Yanagida, Y. Fujimoto, M. Arai, M. Koshimizu, T. Kato, D. Nakauchi, and N. Kawaguchi: *Sens. Mater.* **32** (2020) 1351.
- 19 P. Kantuptim, M. Akatsuka, D. Nakauchi, T. Kato, N. Kawaguchi, and T. Yanagida: *Sens. Mater.* **32** (2020) 1357.
- 20 M. Akatsuka, D. Nakauchi, T. Kato, N. Kawaguchi, and T. Yanagida: *Sens. Mater.* **32** (2020) 1373.
- 21 D. Nakauchi, T. Kato, N. Kawaguchi, and T. Yanagida: *Sens. Mater.* **32** (2020) 1389.
- 22 Y. Takebuchi, H. Fukushima, T. Kato, D. Nakauchi, N. Kawaguchi, and T. Yanagida: *Sens. Mater.* **32** (2020) 1405.
- 23 H. Kimura, T. Kato, D. Nakauchi, N. Kawaguchi, and T. Yanagida: *Sens. Mater.* **32** (2020) 1381.
- 24 T. Kato, D. Nakauchi, N. Kawaguchi, and T. Yanagida: *Sens. Mater.* **32** (2020) 1411.
- 25 N. Kawaguchi, G. Okada, Y. Futami, D. Nakauchi, T. Kato, and T. Yanagida: *Sens. Mater.* **32** (2020) 1419.
- 26 D. Maruyama, S. Yanagisawa, Y. Koba, T. Andou, and K. Shinsho: *Sens. Mater.* **32** (2020) 1461.
- 27 R. Oh, S. Yanagisawa, H. Tanaka, T. Takata, G. Wakabayashi, M. Tanaka, N. Sugioka, Y. Koba, and K. Shinsho: *Sens. Mater.* **33** (2021) 2129.
- 28 D. Shiratori, T. Kato, D. Nakauchi, N. Kawaguchi, and T. Yanagida: *Sens. Mater.* **33** (2021) 2171.
- 29 H. Kimura, T. Kato, D. Nakauchi, N. Kawaguchi, and T. Yanagida: *Sens. Mater.* **33** (2021) 2187.

- 30 H. Masai, T. Ina, H. Kimura, N. Kawaguchi, and T. Yanagida: *Sens. Mater.* **33** (2021) 2155.
- 31 T. Kato, D. Shiratori, M. Iwao, H. Takase, D. Nakauchi, N. Kawaguchi, and T. Yanagida: *Sens. Mater.* **33** (2021) 2163.
- 32 T. Yanagida, Y. Fujimoto, H. Masai, G. Okada, T. Kato, D. Nakauchi, and N. Kawaguchi: *Sens. Mater.* **33** (2021) 2179.
- 33 N. Kawaguchi, H. Masai, M. Akatsuka, D. Nakauchi, T. Kato, and T. Yanagida: *Sens. Mater.* **33** (2021) 2215.
- 34 D. Shiratori, D. Nakauchi, T. Kato, N. Kawaguchi, and T. Yanagida: *Sens. Mater.* **32** (2020) 1365.
- 35 F. W. K. Firk, G. G. Slaughter, and R. J. Ginther: *Nucl. Instrum. Methods* **13** (1961) 313.
- 36 M. Koshimizu, K. Iwamatsu, M. Taguchi, S. Kurashima, A. Kimura, T. Yanagida, Y. Fujimoto, K. Watanabe, and K. Asai: *J. Lumin.* **169** (2016) 678.
- 37 S. W. S. McKeever, S. Sholom, and N. Shrestha: *Radiat. Meas.* **123** (2019) 13.
- 38 W. Zhou, G. Wang, X. Zheng, L. Yu, J. Zhang, Z. Qiu, and S. Lian: *J. Am. Ceram. Soc.* **102** (2019) 5890.
- 39 Y. Zhang, Z. Zhu, and Y. Qiao: *Mater. Lett.* **93** (2013) 9.
- 40 Y. Hao and J. Cao: *Phys. B: Condens. Matter* **493** (2016) 68.
- 41 N. Kawaguchi and T. Yanagida: *Sens. Mater.* **31** (2019) 1257.
- 42 H. Masai, H. Kimura, N. Kawaguchi, T. Yanagida, and N. Kitamura: *Radiat. Meas.* **135** (2020) 106344.
- 43 H. Masai, Y. Yamada, Y. Suzuki, K. Teramura, Y. Kanemitsu, and T. Yoko: *Sci. Rep.* **3** (2013) 3541.
- 44 D. Shiratori, H. Kimura, D. Nakauchi, T. Kato, N. Kawaguchi, and T. Yanagida: *Radiat. Meas.* **134** (2020) 106297.
- 45 T. Yanagida, K. Kamada, Y. Fujimoto, H. Yagi, and T. Yanagitani: *Opt. Mater.* **35** (2013) 2480.
- 46 T. Yanagida, Y. Fujimoto, T. Ito, K. Uchiyama, and K. Mori: *Appl. Phys. Express* **7** (2014) 062401.
- 47 T. Yanagida, Y. Fujimoto, N. Kawaguchi, and S. Yanagida: *J. Ceram. Soc. Japan* **121** (2013) 988.
- 48 N. Kawaguchi and T. Yanagida: *Jpn. J. Appl. Phys.* **59** (2020) SCCB21.
- 49 D. Nakauchi, G. Okada, Y. Fujimoto, N. Kawano, N. Kawaguchi, and T. Yanagida: *Phys. Chem. Glas. Eur. J. Glas. Sci. Technol. Part B* **60** (2019) 10.
- 50 T. Yanagida: *Proc. Japan Acad. Ser. B* **94** (2018) 75.
- 51 A. J. J. Bos: *Radiat. Meas.* **41** (2006) S45.
- 52 Y. Isokawa, H. Kimura, T. Kato, N. Kawaguchi, and T. Yanagida: *Opt. Mater.* **90** (2019) 187.
- 53 M. Iwao, H. Takase, D. Shiratori, D. Nakauchi, T. Kato, N. Kawaguchi, and T. Yanagida: *Radiat. Meas.* **140** (2021) 106492.